3D Numerical Modeling of Flow Field and Flushing Channel Formation in Reservoirs

AUTHOR(S):

ESMAEILI, Taymaz; SUMI, Tetsuya; KANTOUSH, Sameh A.; KUBOTA, Yoji

CITATION:

ESMAEILI, Taymaz ...[et al]. 3D Numerical Modeling of Flow Field and Flushing Channel Formation in Reservoirs. 京都大学防災研究所年報. B 2014, 57(B): 468-482

ISSUE DATE:

2014-06

URL:

http://hdl.handle.net/2433/196116

京都大学防災研究所年報 第 57 号 B 平成 26 年 6 月
Annuals of Disas. Prev. Res. Inst., Kyoto Univ., No. 57 B, 2014

3D Numerical Modeling of Flow Field and Flushing Channel Formation in Reservoirs

Taymaz ESMAEILI[(1)], Tetsuya SUMI, Sameh A. KANTOUSH[(2)] and Yoji KUBOTA[(3)]

(1) Department of Urban Management, Graduate School of Engineering, Kyoto University
(2) Department of Civil Engineering, German University in Cairo (GUC)
(3) Hydro-soft Technology Institute Co., Ltd.,

Synopsis

Flushing with water level drawdown is one of the proposed methods for preserving the storage capacity of dam reservoirs. The accelerated shallow flow pattern during the sediment flushing increases the induced bed shear stress and then the deposited sediment in the dam reservoir would be eroded. Thus, Shallow flow condition which is characterized by its complex mixing process and inherent dynamic nature plays major role in draw down flushing process. In the present study a fully three-dimensional numerical model that employs the Finite Volume Approach (FVM) was utilized to reproduce the 3D flow field in various shallow reservoir geometries with fixed and deformed equilibrium bed. Afterwards, the model with wetting/drying algorithm and adaptive mesh which moves in accordance to water and bed level changes was employed to simulate the sediment flushing process of Dashidaira reservoir. The total volume of flushed out sediment and bed deformation after flushing compared with the observations. Numerical outcomes show that the model could reproduce many aspects of the complex procedure of flushing process and a reasonable agreement was found between the numerical outcomes and observations.

Keywords: Shallow flows, Reservoir management, 3D numerical simulation, free-flow sediment flushing

1. Introduction

Sediment deposition is the principal problem affecting the useful life of reservoirs. A decreased storage volume reduces the reservoir function for flood control purpose, electricity production and water supply. Furthermore, the sediment yields of the Japanese rivers are high in comparison with other countries due to the topographical, geological and hydrological conditions (Sumi, 2006). Among several techniques, the flushing and sluicing plays an important role in the sediment removal and reduction, as they are efficient hydraulic sediment removal technique to restore the reservoir storage capacity. During the flushing with drawdown, bottom outlets are opened and water level is lowered to generate and accelerate the unsteady flow towards the outlet (Morris & Fan, 1998). This process will initiate the progressive and retrogressive erosion pattern in tail and delta reaches of the reservoirs respectively (Battuca, 2000). Many reservoirs are not flushed because an accurate prediction of the success of an upcoming reservoir flushing is time and cost-intensive (Haun

& Olsen, 2012). Loss of the stored water besides the lack of knowledge about the amount of the flushed out sediment and location of the erosion-deposition area in the reservoir will be the negative factors for choosing the free-flow sediment flushing. Following that, the environmental effects downstream of the reservoir caused by the flushing are difficult to estimate because of the complexity of free-flow sediment flushing process. So, it is important to have an initial assessment of the efficiency of upcoming free-flow sediment flushing. Numerical models were developed as an alternative over the last decades to avoid scaling problems of physical models and also because of an expected time and cost reduction (Chandler et al., 2003). Three-dimensional numerical models are still under development for application in this field. Atkinson (1996), Khosronejad (2008), Haun & Olsen (2012), Esmaeili et al. (2014) used three-dimensional models for simulating the flushing process in the physical model scale. Application of three-dimensional numerical models for simulating the complex structure of interacting flow and sediment field would be useful for understanding the different stages of flushing process and utilize the outcomes for application in the prototype scale.

Free-flow sediment flushing through dam reservoirs is one of the typical techniques in Japan because of sufficient rain fall, economical advantages, independency from other facilities and potential for high efficiency. During the free-flow state, after lowering the water level, the shallow flow plays major role in sediment transportation pattern and bed deformation (i.e. flushing channel formation) in reservoir. Therefore, it is necessary to be familiar with the behavior of shallow waters characteristic. Shallow waters are defined as a flow field in which the vertical dimension of fluid domain is significantly smaller than its horizontal dimensions (Yuce & Chen, 2003). This type of flows is prominent in the nature and also emerges in various engineering applications including sudden expansions (Shapira et al., 1990), compound channels (Ghidaoui & Kolyshkin, 1999 and Chu et al., 1991), storage chambers (Adamson et al., 2003), settling tanks (Frey et al., 1993) as well as shallow reservoirs sedimentation (Kantoush et al., 2008a & 2010a).

The sediment transportation pattern in shallow reservoirs is seriously affected by large-scale transverse motions and turbulent coherent structures. Therefore, measurement of 2D surface velocity and vertical velocity components with high spatial resolution would be necessary to predict the favorable sedimentation zone. Such kind of knowledge would be interesting for more efficient sediment management strategies in the reservoirs. In addition, assessments of the flow field within a shallow reservoir is necessary for characterizing the flow domain such as location of main jet flow, reverse flow and eddies.

Kantoush (2007) presented a comprehensive review of experimental tests in shallow reservoirs with transverse flow motions in symmetric channel expansions. The observations revealed that asymmetric flow pattern can be developed under a certain geometric and hydraulic condition even if the symmetric geometry and hydraulic condition is employed. Same outcome has been obtained by Adamson et al. (2003) and Stovin & Saul (1996) regarding the storage tank sedimentation and storage chambers, respectively. However, most of the studies in the literature considered the sudden plane expansions of an infinite length and studies focusing on various geometric and hydraulic parameters are very limited. Dewals et al. (2008) and Dufresne et al. (2011) used 2D numerical models to investigate the flow pattern distribution in shallow reservoirs. Nevertheless, the one and two dimensional models are not able to directly simulate the secondary current influences in complex 3D flows, especially on deformed beds due to the complexity of this type of flow fields.

In the present study, first, flow pattern and the potential instabilities in diverse shallow reservoir geometries with different length-to-width (Aspect ratio that is called AR) and reservoir width to inlet channel width (Expansion ratio that is called ER) were considered for numerical simulations. The fixed bed and also equilibrium bed after free-flow flushing were used as the initial bed condition as well.

Numerical outputs were compared with the experimental measurements of surface velocity by Large Scale Particle Image Velocimetry (LSPIV) for all cases as well as 3D velocity component for

one case. Besides the good agreement between the measured and simulated flow velocity field, numerical model could reproduce the steady asymmetric flow pattern when a perturbation quantifier was employed.

Afterwards, the free-flow sediment flushing event which was performed during a flood event in Dashidaira reservoir in Japan was modeled to assess the bed topography changes in different stages of sediment flushing process. The cross sections in a specific segment of the reservoir were compared with the measurements. Results show that model could reproduce the main governing aspects of the sediment flushing event in a real prototype scale. However, +50/-50 percent differences between the measurement and simulation result in the real prototype scale is not uncommon especially when the geometry is complex and uncertainty exists in the data collection.

2. Material and methods

2.1 Three dimensional numerical model

Fully 3D numerical model SSIIM was employed in this study. The numerical model solves the mass conservation and Reynolds-averaged Navier-Stokes equation in three dimensions (Equation 1 and 2) to compute the water motion for turbulent flow as follows.

$$\frac{\partial U_i}{\partial x_i} = 0 \tag{1}$$

$$\frac{\partial U_i}{\partial t} + U_j \frac{\partial U_i}{\partial x_j} = \frac{1}{\rho}\frac{\partial}{\partial x_j}\left(- P\delta_{ij} + \rho \upsilon_T (\frac{\partial U_i}{\partial x_j} + \frac{\partial U_j}{\partial x_i}) \right) \tag{2}$$

in which i=1, 2, 3 is the representative of three directions; where U_i is the averaged velocity, x is the spatial geometrical scale, ρ is the water density, P is the Reynolds-averaged pressure, δ_{ij} is the Kronecker delta and v_T is the turbulent eddy-viscosity. For transforming the partial equations into algebraic equations, the finite volume method is applied as discretization method, together with the second order upwind scheme.

The change in water-levels was based on calculated pressure field. The pressure was extrapolated to the water surface and the pressure difference between a surface node and the downstream node was used to estimate the water elevation difference (Olsen, 2013). The turbulence is modeled by the standard k-ε model, using constant empirical values (Launder & Spalding, 1972). The unknown pressure field is calculated employing Semi Implicit Method for Pressure-Linked Equations, (SIMPLE) method (Patankar, 1980). The grid is adaptive and moves with change in the bed and water levels.

The Dirichlet boundary condition for the water inflow (logarithmic velocity distribution) was used while for the water and sediment outflow zero-gradient boundary condition was specified. For the boundary condition at the walls, where there is no water flux, the empirical wall laws introduced by Equation 3 were used:

$$\frac{U}{u^*} = \frac{1}{\kappa}\ln\left(\frac{30y}{k_s}\right) \tag{3}$$

where the shear velocity is denoted u^*, κ is the Karman constant equal to 0.4, y is the distance to the wall and k_s is the equivalent roughness.

The sediment transport computation for simulating the morphological change is divided into suspended and bed load transport. Suspended load is calculated by solving the transient convection-diffusion equation formula (Equation 4) and the default empirical formula computing the bed load is Van Rijn formula (Equation 5)(VanRijn, 1984a). In addition, Meyer-Peter-Muller bed load transport formula has been implemented in numerical model (Equation 6). This formula is more appropriate than others for steep rivers in which the sediment load transportation is mainly bed load (i.e Kurobe river). The latter formula has been examined in European rivers and sediment flushing in Bodendurf reservoir, Austria (Haun et al., 2012)

$$\frac{\partial c}{\partial t} + U_j \frac{\partial c}{\partial x_j} + w\frac{\partial c}{\partial z} = \frac{\partial}{\partial x_j}(\Gamma_T \frac{\partial c}{\partial x_j}) \tag{4}$$

Where U is the water velocity, w is the fall velocity of sediments, Γ is the turbulent diffusivity and can be expressed by (Equation 7) and c is the sediment concentration over time t within the spatial geometrical scales x and z.

Numerical model uses an unstructured adaptive grid and only the flow phase (water body) is modeled. Since wetting/drying algorithms were

implemented to avoid emerging distorted cells, number of cells in spatial directions can vary during the computation. Thus, it is necessary to introduce the boundary values for wetting/drying algorithm. In this paper for simulation of sediment flushing event, z_1= 0.3m (lower boundary) and z_2= 1m were used. In areas with a water depth shallower than 0.3m no cell would be generated and the area will be dried up (The area disappears from the computational grid). In areas with water depth between 0.3m and 1m one cell is produced and a two-dimensional computation is conducted while the various numbers of cells along the vertical direction is generated in areas with the water depth higher than 1m. In the latter case, the vertical cell numbers is an exponential function of the ratio of local water depth to the maximum water depth.

$$\frac{q_{b,i}}{d_i^{1.5}\sqrt{\frac{(\rho_s-\rho_w)g}{\rho_w}}} = 0.053\frac{\left[\frac{\tau-\tau_{c,i}}{\tau_{c,i}}\right]^{1.5}}{d_i^{0.3}\left[\left(\frac{(\rho_s-\rho_w)g}{\rho_w v^2}\right)\right]^{0.1}} \quad (5)$$

where $q_{b,i}$ is sediment transportation rate for the *i*th fraction of bed load per unit width, d_i is the diameter of the *i*th fraction, τ is the shear stress, $\tau_{c,i}$ is the critical shear stress for d_i which was calculated from the Shield's curve, ρ_s is the density of sediment, ρ_w is the density of the water, g is the gravity acceleration and v is the kinematic viscosity.

$$q_{b,i} = \frac{1}{g}\left[\frac{\rho_w grI - 0.047g(\rho_s-\rho_w)d_{50}}{0.25\rho_w^{\frac{1}{3}}\left(\frac{\rho_s-\rho_w}{\rho_s}\right)^{\frac{2}{3}}}\right] \quad (6)$$

In Meyer-Peter-Muller bed load formula d_{50} is the characteristic sediment size, I is the slope of the energy line and r is the hydraulic radius.

$$\Gamma_T = \frac{\nu_T}{Sc} \quad (7)$$

where Sc is the Schmidt number representing the ratio of eddy viscosity coefficient ν_T to diffusion coefficient and set to 1.0 as default.

In order to compute the suspended sediment concentration in the cells close to the bed Equation 8 was used as boundary condition (Van Rijn, 1984b).

$$C_{bed} = 0.015\frac{d_i^{0.3}}{a}\frac{\left[\frac{\tau-\tau_{c,i}}{\tau_{c,i}}\right]^{1.5}}{\left[\frac{(\rho_s-\rho_w)g}{\rho_w v^2}\right]^{0.1}} \quad (8)$$

where a is the distance reference level and set equal to roughness height.

2.2 Experimental setup for flow field modeling in shallow reservoirs

The experimental tests were carried out at the Laboratory of Hydraulic Constructions of Swiss Federal Institute of Technology (EPFL) in a rectangular reservoir with the maximum inner length (L) of 6m and width (B) of 4m (Kantoush, 2007). Also, the inlet and outlet rectangular channel width (b) and length (l) were 0.25m and 1m respectively. Both channels were installed at the center of upstream and downstream side wall of the reservoir. The different shallow reservoir geometry achieved experimentally by moving the PVC plate walls. The reservoir depth is 0.3m and the both side walls and bottom is hydraulically smooth and flat. The water level in the reservoir was controlled by a 0.25m width and 0.3m height flap gate set up at the end of outlet channel. A moveable frame with 4m length was mounted on the side walls of the reservoir for installing the measurement devices. Table 1 shows geometrical attributes of four geometries employed in the present study. As for the geometrical parameters, ER=B/b shows the influence of change in the reservoir width while AR=L/B is appropriate for describing the effect of variations in the reservoir length (Dewals et al., 2008).

Large Scale Particle Image Velocimetry technique (LSPIV) was used for measuring the surface velocity field. Ultra Sonic Velocity Profiler device (UVP) was employed for providing the 3D flow velocity measurements as well. Also, within the frame work of experimental study, sedimentation and sediment flushing from the shallow reservoirs were investigated (Kantoush et al., 2008b). Non-uniform crushed walnut shells were used as suspended load in sedimentation and flushing tests. The median size of this non-cohesive

light-weight and homogenous grain material was 50 μm with σ_g of 2.4 and a density of 1500 kg/m³. The flow discharge rate (Q) and water depth (h) were constant for all experiments as 0.007m³/s and 0.2m respectively except for cases with deformed equilibrium bed. Thus, in all tested configurations with fixed bed, the measured Froude and Reynolds number at the inlet channel were kept constant as Fr=0.1 and $Re=1.75\times10^4$ respectively. In case of measurements of flow field on deformed bed after flushing, the water level and discharge were 0.1m and 0.007m^3/s respectively.

Figure 1 illustrates the observed flow streamlines for case T8 and T13. As can be observed, the issuing flow jet deviated to the right hand side which forms asymmetric flow pattern in case T8. Also, symmetric flow pattern with one main jet trajectory in the centerline and two side eddies has been developed for case T13. Kantoush (2007) concluded that the deviation to the right hand side is due to the random disturbance of the initial boundary condition and a mirror situation would be easily established by slight disturbance in the boundary condition. The flow deviation to one side of the reservoir corresponds to the increase of flow velocity in one side of the jet and consequent reduction of the pressure. This process will produce the flow deviation to one side of the reservoir and called Coanda effect (Chiang et al., 2000).

Table 1. Geometrical parameters of the reservoirs

Case	L(m)	B(m)	Pr(m)*	ER	AR	SF**
T 8	6	2	15.5	8	3	0.375
T 9	6	1	13.5	4	6	0.122
T 11	5	4	17.5	16	1.25	0.99
T 13	3	4	13.5	16	0.75	0.97

*Pr is the wetted perimeter.
** A is the total reservoir area and SF is the shape factor defined as $(A/Pr^2)\times ER$.

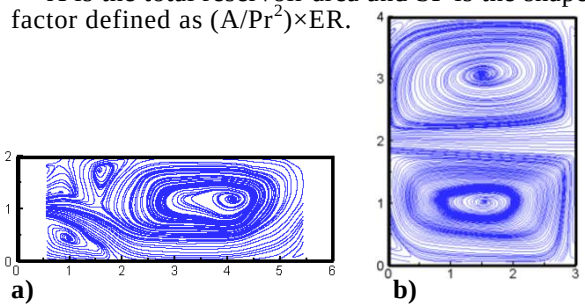

Fig. 1 Observed streamlines of the surface flow field for a) case T8 and b) case T13.

2.3 Case study description: Dashidaira reservoir, Kurobe River, Japan

Kurobe River located in the eastern part of the Toyama prefecture. The river originates from the Washibadake Mountain and then extends to the plain area at the Aimoto point which is 13km upstream of the coastal area of Japan Sea. The Catchment area of the Kurobe River is 682 km^2 and the length of the river is 85km. River bed is steep and the bed slope varies between 1% and 20%. The dominant sediment type is weathered granite and owing to the steep valleys and consequent sand slides the sediment production potential is very high in this river basin (Minami et al., 2012). The annual rainfall in the mountain area of the basin is 4000mm (PWRI, 1993). Dashidaira dam with 76.7m height has been constructed in 1985 by Kansai Electric Company over the Kurobe River that has the highest sediment concentration among the rivers in Japan. This dam provides 124MW hydroelectric power. Also, this dam has been equipped with bottom outlet facilities to flush out the deposited sediment in the reservoir. The gross and effective storage capacity of the dam reservoir is 9.01 and 1.66 MCM respectively. Until year 2000 50% of the gross storage capacity and 29% of the effective storage capacity was filled due to the sedimentation.

The sediment flushing operation has been performed since 1991. From June 2001 the coordinated sediment flushing in both Dashidaira and Unazuki reservoir, which is 7 km downstream of Dashidaira dam, is ongoing (Liue et al., 2004). Coordinated sediment flushing is executed at the first major flood event every year and the sediment sluicing is done at the successive bigger ones by the same reservoir operation to prevent additional sediment deposit in the reservoir (Sumi, 2006). Figure 2 illustrates the location of Dashidaira reservoir in Kurobe River Basin. Although Dashidaira reservoir is a narrow shaped, there are local wide segments. Figure 3 shows the topographic map of Dashidaira reservoir which was extracted from the surveying data before the sediment flushing operation in 2012.

As for the coordinated sediment flushing, if the flood satisfies a stipulated standard, both reservoirs water level is lowered based on the instructions to increase the induced bed shear stress. As a result the

incoming sediment and deposits in the reservoirs are flushed out through the sediment flushing gates to downstream channel (Minami et al., 2012). Figure 4 demonstrates the sediment flushing through the Dashidaira reservoir during the free-flow state.

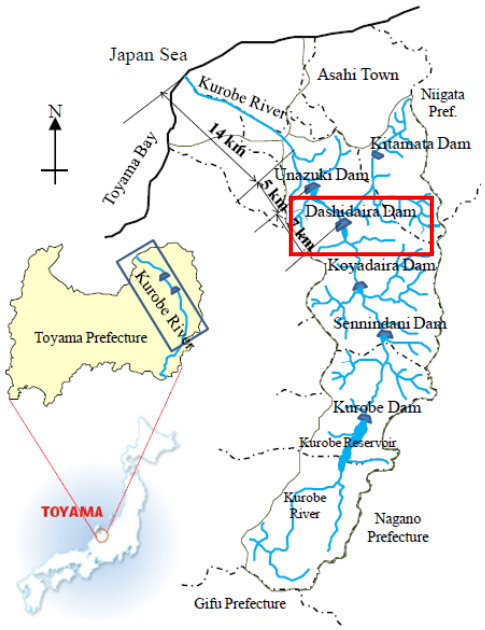

Fig. 2 Location of Dashidaira and Unazuki reservoir in Kurbe River Basin (Kantoush et al., 2010b).

Nowadays, sediment flushing operation in the Kurobe River is aimed to keep a constant bed form without trapping sediment in the reservoir as much as possible by executing the flushing within the

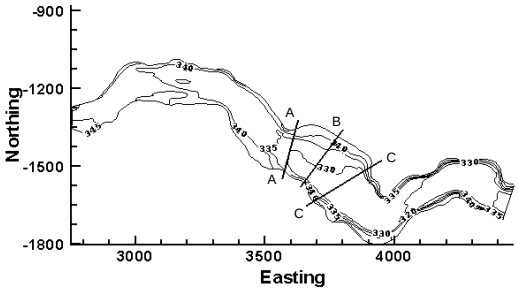

Fig. 3 Topography of Dashidira reservoir before flushing event in May 2012 and considered cross sections for further quantitative assessment.

natural flood events between June and August. As a result, the water quality deterioration such as happened in the 1991 sediment flushing event, has not occurred recently. The mentioned approach also contributed in preserving the storage capacity of Dashidaira and Unazuki reservoir noticeably.

Fig. 4 Aerial photo from free-flow sediment flushing at Dashidaira Reservoir.

2.3.1. Data collection

Due to the importance of bed level assessment in Dashidaira reservoir for sustainable sediement management, three times annual bed changes measurement are done in the reservoir (i.e. before and after flushing). The bed level measurements before flushing were employed to prepare the initial bed topography of the reservoir.

The water level at the dam site as well as the Inflow and outflow discharge is recorded during the free-flow sediment flushing operation with the 60 minutes intervals. These data were utilized as the hydrodynamic boundary condition to introduce the water level draw-dawn procedure as well as discharge changes to the numerical model. Figure 5 shows the water level and discharge fluctuations during the free-flow sediment flushing operation event in June 2012.

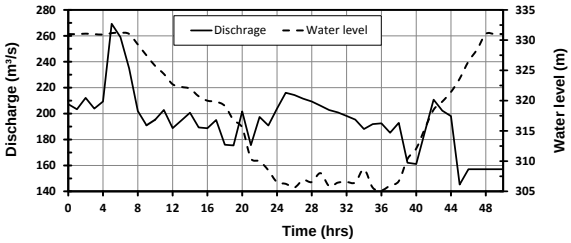

Fig. 5 Water level and discharge rates during the flushing operation in June 2012.

The grain size distribution of the bed materials in the reservoir was determined based on the taken onsite samples. The sorting process of the bed material sizes in the reservoir can be clearly

observed. While d_{50} of the sediment at the entrance area of the reservoir was in the range of 32mm-76mm (very coarse gravel and cobble), the d_{50} decreased to less than 0.5mm in downstream areas. Bed material size distribution within the reservoir area was obtained based on the size interpolation of the available bed material samples.

7 sediment size fractions were considered that is ranged between 0.374mm and 316mm. The density of the sediment determined 2.65gr/cm^3 while the porosity assumed to be in the range of 50%-70%.

The free-flow sediment flushing event in June 2012 was a special case in which the major sediment inflow from the upstream boundary was wash load. Wash load is basically assumed to be transported without deposition in the reservoir because of their small size that is mainly in the range of clay and silt. Moreover, a reliable wash load measurement when the water level and discharge fluctuates during the free-flow sediment flushing is scarce. Thus, in the sediment transportation process (i.e. erosion & deposition) in the reservoir, wash load effect was neglected.

3. Results & Discussions

3.1 Numerical model ability to represent instabilities in flow field

Simulations have been carried out by employing the geometry and inflow/outflow condition of the experimental model. The k-ε turbulence model was employed and numerical runs were done until a steady-state flow condition is achieved.

Based on the experimental measurements computational mesh for all reservoir geometries were made. The mesh cell size for case T8, T9, T11 and T13 in X and Y direction was 5cm × 1.5cm, 5cm × 2.5cm, 5cm × 2cm and 2.5cm × 1cm respectively. Considering the 11 cells for vertical grid distribution, the total number of cells over the main reservoir geometry were 174460, 52800, 220000 and 528000 respectively.

Simulations showed that the model was not able to reproduce an asymmetric flow pattern when the geometry configuration and hydraulic boundary condition are completely symmetric. This is owing to the implemented mathematical algorithms which were not aimed to reproduce such kind of artificial numerical results.

In order to have such kind of asymmetric flow pattern, slight disturbance in the inlet boundary condition was implemented for all runs and non-uniform cross-sectional velocity distribution was utilized in the inflow boundary condition. Thus, the initial velocity magnitude in one side of the inlet channel differs 2.5% in comparison to the other side in all cases. Such kind of disturbance is an unavoidable phenomenon in the physical modeling. This small perturbation of the inflow condition will impose significant effect on the flow field of narrow reservoirs (i.e. case T9) in the numerical model. This would be because of the unstable nature of symmetric flow in such geometries which reveals the high sensitivity of the flow pattern to the inflow boundary condition.

Time step was calibrated as 2 seconds for run T8 and T9 whereas it was 0.5 second for T11 and T13 in the numerical simulation. In case of flow field simulation on the equilibrium deformed bed, the bed roughness was fixed as 0.00015m which equals to 3 times the median sediment size.

Figure 6 shows the simulated and measured surface velocity magnitudes (V) in m/s and flow distribution pattern. As can be clearly observed from Figure 6, asymmetric flow pattern has developed in case T9 whereas symmetric flow pattern is seen for case T13. The model could simulate the surface flow velocity pattern almost similar to the measured one by reproducing the dominant aspects such as the main flow jet trajectory and location of the reverse flow as well as the main vortices and corner gyres. Nonetheless, numerical model outcomes show the straighter and longer reverse flow trajectory than observations in both cases. Consequently, size of the upstream corner gyres in the numerical outputs is smaller than the experimental observations.

Figure 7 illustrates the simulated streamwise and transversal surface velocity distribution versus the measured one in the middle cross-section of case T9 & T13. Outputs reveal that the numerical model results are globally consistent with the observations. However, small discrepancy between the simulation results and measurements is due to the concentrated flow pattern and lower diffusion of the main jet as well as the reverse flow in the numerical model

outcomes.

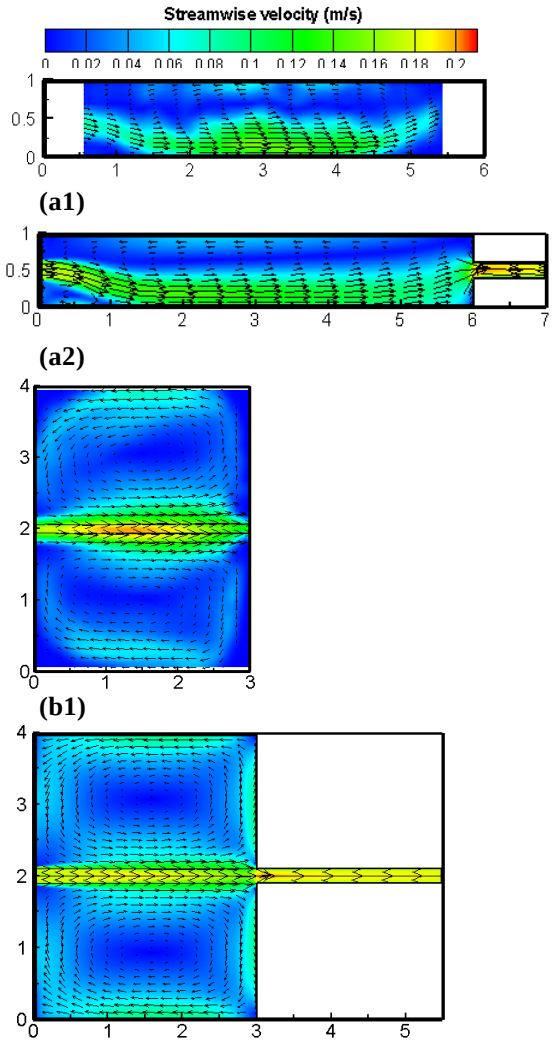

Fig. 6 Measured surface velocity field with velocity vectors for runs (a1) T9 and (b1) T13; Corresponding simulated velocity field for runs (a2) T9 and (b2) T13.

The vertical distribution of flow velocity field is also important for assessing the sediment transport in reservoirs. Thus, the numerically simulated 3D flow velocity field was compared with the measured 3D velocity components provided by the UVP. Figure 8a and 8b demonstrates the longitudinal velocity distribution over the flow depth, at upstream, middle, and downstream area of case T9. It can be seen that the higher longitudinal velocity has been deflected towards the right bank side and the reverse flow is reproduced beside the left bank side. Such kind of change in the flow direction across the reservoir is also qualitatively consistent with the experimental observations. Compared with the experimental measurements, numerical model overestimates the longitudinal velocity magnitudes. Furthermore, numerical model results reveal a more uniform distribution of longitudinal velocity in vertical and lateral direction than measurements.

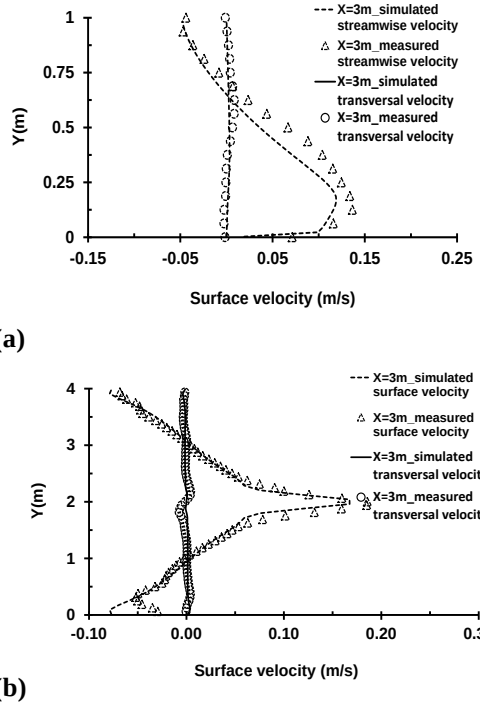

Fig. 7 The measured streamwise and transversal surface velocity along the middle cross section of the reservoirs versus the simulated surface velocity for (a) T9 and (b) T13.

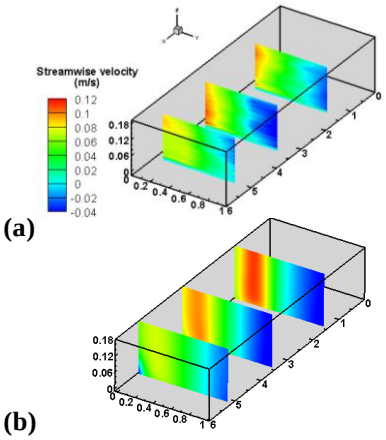

Fig. 8 (a) The UVP measurements of the longitudinal velocity over the flow depth at x=1.5m, 3.5m and 5.2m; (b) the corresponding simulated velocity.

3.2 Flow field simulation on deformed beds

The final bed morphology, which was obtained after the sediment flushing, was introduced to the model as the boundary condition and then three-dimensional flow field was calculated. This information would be useful for flood risk

assessment especially in reservoirs near the urban areas.

Flow field calculation on a deformed bed is much more complex than that of on the fixed bed owing to the shallower flow condition with higher velocity components on the existing friction of bed forms. The final deformed bed after sediment flushing in case T8 and T11 has been shown in Figure 9. Figure shows that the flushing channel has shifted to the left side of the reservoir in case of T8. Figure 10 also illustrates the measured surface velocity after flushing by LSPIV technique versus the simulated one for case T8 and T11. As can be clearly observed, model reproduced the surface velocity pattern similar to the observed one in case T8 while it was different in case T11. In case T11, the main and reverse jet trajectory is narrower and straighter than that of the measured one. Moreover, slight disturbance in the boundary condition was not considered in the model for the current cases.

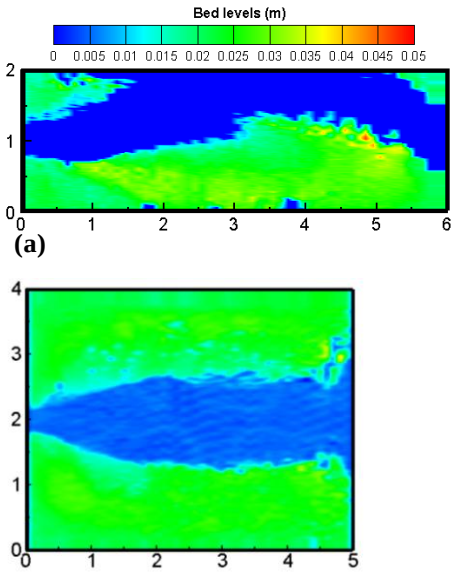

(a)

(b)

Fig. 9 Equilibrium deformed bed after flushing for (a) case T8 and (b) case T11.

Figure 11 demonstrates the quantitative comparison between the measured surface velocity by LSPIV and the simulated one for case T8 in the middle cross-section.

3.3 Numerical modeling of flushing channel formation in Dashidira reservoir

The modeled bed level changes after the flushing were validated with the measured data after the flushing event in June 2012.

Since Dashidaira reservoir has been located in a steep mountainous region with high sediment

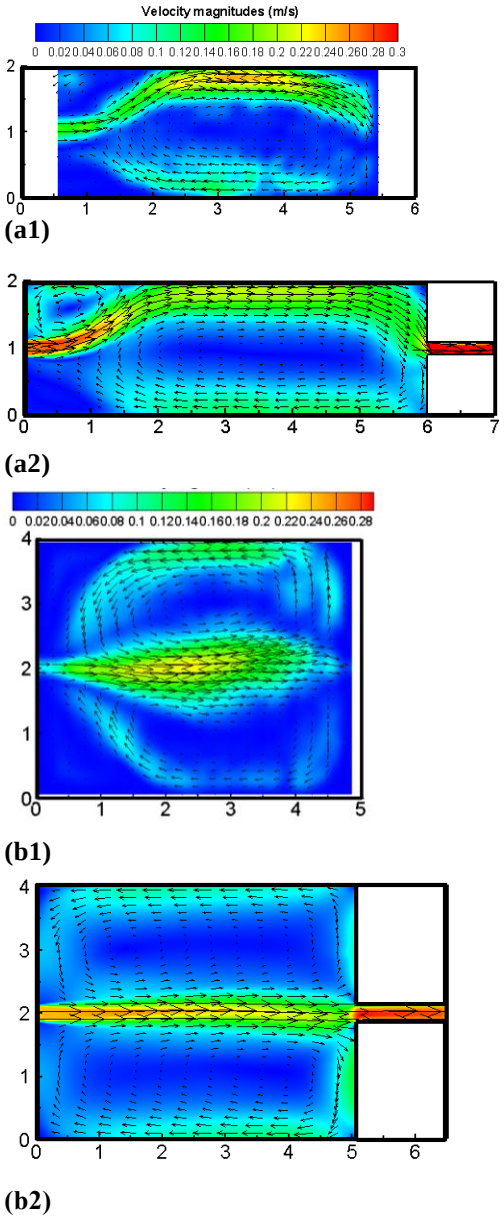

(a1)

(a2)

(b1)

(b2)

Fig. 10 Measured surface velocity field with vectors on deformed bed for runs (a1) T8 and (b1) T9. Corresponding simulated velocity field for runs (a2) T8 and (b2) T11.

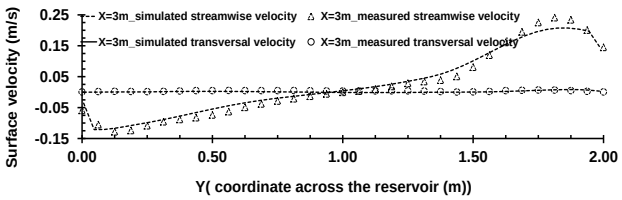

Fig. 11 Measured surface velocity field versus the simulated one for case T8.

transportation in the bed load form, the Meyer-Peter-Mueller sediment transportation formula was employed. Due to the implicit free-water surface algorithm in which the computed pressure field is used for updating the water surface, large time steps can be utilized for numerical simulations. Consequently, time step of 10 seconds was selected and the active sediment layer thickness adjusted to 1 m in the model. The angle of repose for the sediment ranged between 30°-32° and value of 32° was applied in the sand slide algorithm. As to the hydrodynamic boundary condition, water level and discharge rates in Figure 5 were introduced to the model and numerical results were presented.

Second order upwind scheme (SOU) was employed in numerical modeling since it can handle more complex flow field than first order power law scheme (POW), especially in the channel bending, where the secondary currents play major role in erosion and deposition pattern (Haun & Olsen, 2012). Figure 12(a) illustrates the measured bed levels before flushing. In Figure 12(b) and 12(c), the measured and simulated bed topography after flushing has been shown respectively. Formation of the flushing channel during the free-flow state, similar to the prototype, was observed in the numerical model outcomes as shown in Figure 13.
Regarding the surface flow velocities during the free-flow condition, super critical flows emerged with the Froude number between unity and 1.45 in several sections. Meanwhile, the horizontal flow velocities in the flushing channel increased up to 5.5 (m/s) during the draw down stage (Figure 14). Because of the presence of the air in supercritical flows, the free-water surface is disturbed and subsequently it is very likely to have uncertainty in the outputs of this stage.

As can be seen from Figure 12, in the area close to the dam the measured bed levels are different than measured one (Area I). The simulation results show narrower flushing channel in comparison to the observations. This can be attributed to the complex flow field due to the secondary currents and reverse flow pattern in the wide bending area close to the dam site. Moreover, bed forms (i.e. dunes and anti-dunes) which are developed in this area will increase the complexity of the flow and subsequently the sediment transportation pattern.

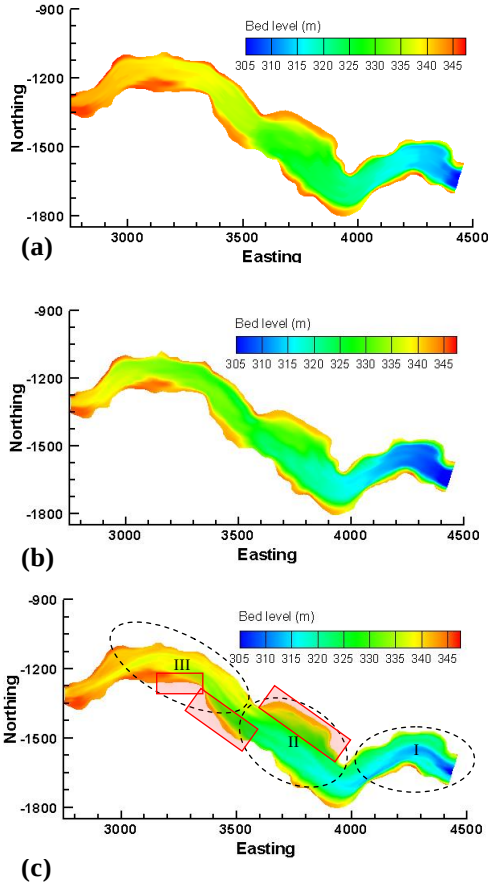

Fig. 12 (a) Measured bed topography of Dashidaira reservoir before flushing; (b) Measured bed levels after flushing, and (c) simulated bed levels.

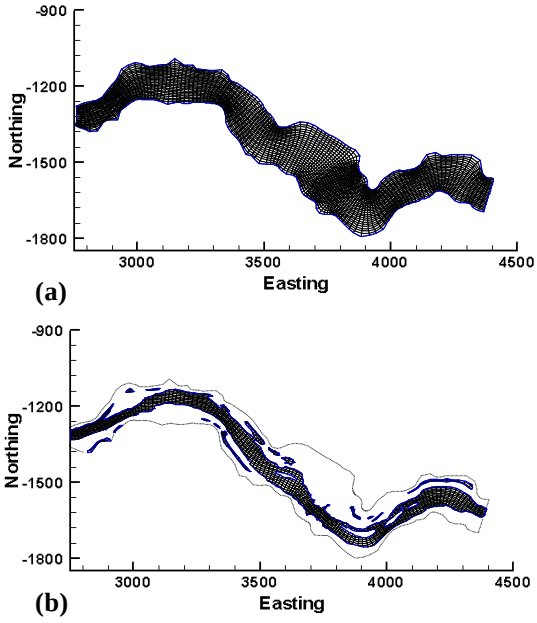

Fig. 13 (a) Computational grid at the beginning of flushing simulation. (b) computational grid during the free-flow condition which shows the flushing channel shape and location.

It should be noted that, numerical model utilizes an empirical formula by Van Rijn (1984c) that is basically developed for small Froude numbers. Thus, it is very likely to simulate different bed forms than that is formed during the sediment flushing process. Moreover, in the areas close to the dam the sediment transport capacity is reached to its highest level that would be smaller than its original value in the prototype. Thus, enough sediment could not be removed from this area and bed levels are different than measured ones. It should be also noted that the complex drawdown procedure is conducted by contribution of spillways and bottom outlets in the prototype. In the numerical model, this procedure has been simplified.

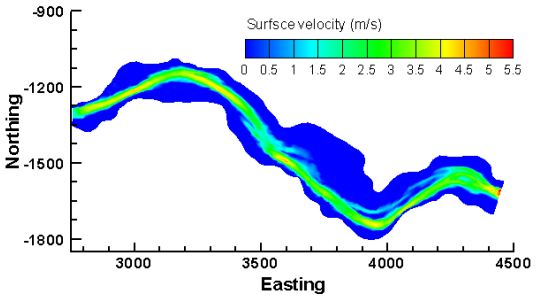

Fig. 14 Simulated flow velocity field in the flushing channel during the free-flow condition.

In Area II, which is the wide middle section of the reservoir, the flushing channel shape and location is more or less consistent with the observations (Fig. 12a-12c). In this area, there is a large amount of deposited sediment. Red hatched rectangles in Figure 12c reveal the regions with high amount of sediment deposition. The flushing channel geometry in Area II has a noticeable contribution in preserving the reservoir storage capacity as well as enhancing the flushing efficiency. Three cross-sections (A-C; Fig. 3) from the outcomes of the numerical model have been presented in Figure 15. In addition, Figure 16 shows the longitudinal profile at the centerline of the reservoir before and after flushing.

During the free-flow flushing operation the narrow flushing channel location is deflected to the right bank region of Area II and consequently there is no chance for erosion of deposited sediment in the left bank region. A large amount of deposited sediment in the form of a big sand bar will remain after flushing operation. Subsequently, application of appropriate measures is likely to increase the volume of sediment evacuation from this segment which may enhance the flushing efficiency. Thus, this study mainly focuses on flushing channel shape, location and geometry within Area II.

Figure 15 clearly shows the bed degradation as well as the flushing channel geometry in Area II. Similar to the measurement, numerical results show that thalweg of the flushing channel has been formed close to the right bank of wide middle section (Area II). This is expected since bed degradation usually occurs along the outer part of the channel bending. In all cross sections, bed degradation has been over estimated in right half of the cross section. Concerning the bed levels in left half, it has been underestimated in case of cross-section A whereas it was more or less consistent with the measurements in cross-section B and C.

In this study, the volume of the eroded sediment from the reservoir was also computed. The total computed volume of the eroded sediment was 308,900 m^3 while it is 408,700 m^3 based on the surveying data. The lower volume of the eroded sediment in numerical simulation is due to the underestimation of the eroded sediment quantity in Area I and II.

As can be observed from Figure 12, the simulated flushing channel width in Area I is narrower than measurements. As for the simulated flushing channel in Area III, the channel could not be propagated enough towards the far upstream region. The reason can be attributed to the type of the bed materials in this area which are mainly coarse gravels. Subsequently model could not simulate the erosion pattern properly in the mentioned region due to the complex velocity profile and effective hydrodynamic forces that is emerged especially during the free-flow state. The other reason is elimination of the cells with shallow water head, from the computational domain, along the left bank of lower part of Area III in where there is a sever bed degradation. It also should be taken into account that the bed measurements is not conducted right after flushing event and also the sediment flushing is conducted in the rainy season in Dashidaira reservoir. Therefore, some

uncertainties would be possible in the bed level measurements because of the dynamic changes in hydrodynamic boundary condition right after the flushing event until the measurements. The other uncertainty is related to the bed material distribution that can have noticeable effect on the accuracy of the numerical model outcomes.

However, the model results are more or less in agreement with the measurements in the main study segment (Area II). An extensive sensitivity analysis on the numerical algorithms and empirical parameters (i.e. in bed load transport formula) in the model will offset the uncertainties to some extent and also result in higher accuracy.

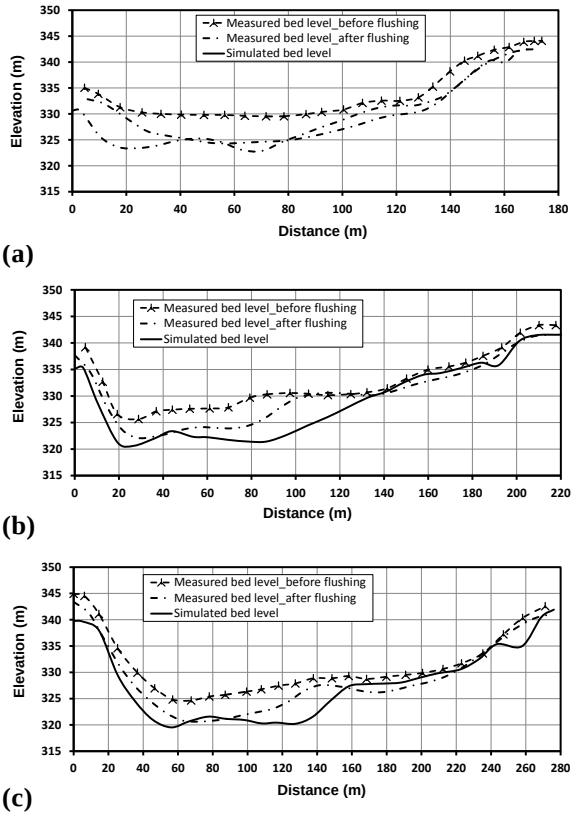

Fig. 15 Bed level changes in (a) cross-section A; (b) cross-section B and (c) cross-section C.

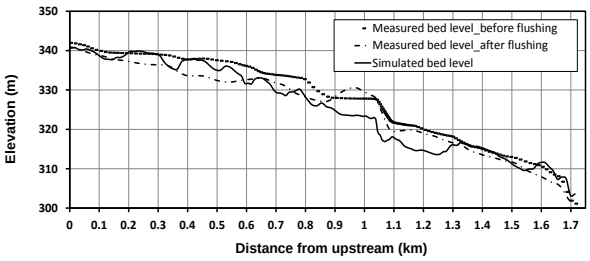

Fig. 16 Longitudinal bed profile at the centerline of the reservoir.

4. Conclusions

Due to the major role of shallow flow condition in flushing channel formation and development during the free-flow state, it is necessary to be familiar with the behavior of such kind of flows. In this paper, first, numerical model SSIIM was utilized for reproducing the 3D velocity field in rectangular shallow reservoirs with different geometries on fixed and deformed bed as well. Measured surface velocity utilizing the LSPIV technique was used for model validation. In addition, 3D velocity components along the flow depth provided by UVP were compared with the numerical results. Afterwards, the numerical model along with wetting/drying algorithm was utilized to model a coupled computation of flow and sediment field in a real prototype scale during a free-flow flushing event. The following outcomes were obtained from this study:

1- Many hydrodynamic aspects such as jet trajectory, recirculation zones, eddies and the flow distribution pattern, in different shallow reservoir geometries were represented by the numerical model. The numerical model also reproduced both symmetric and asymmetric flow pattern in symmetric geometry setup, similar to the observations, by introducing a perturbation in the inflow boundary condition. The numerical outcomes were in good agreement with the experimental observations. However, there was some discrepancy for reproducing the upstream vortex dimension due to the longer concentrated flow and reverse flow jet pattern with lower flow diffusion in the numerical outcomes.

2- The numerical model could successfully show the effect of geometry on the flow pattern. More specifically, the numerical model showed that the flow pattern in geometries with higher SF (i.e. T13) is insensitive to the small disturbance in the inflow condition and the numerical model converged to the steady symmetric flow pattern. On the contrary, calculated flow pattern in geometries with lower SF (i.e. T9) converged to the steady asymmetric flow pattern due to the slight disturbance in the inflow boundary condition. In prototype scale reservoirs with narrow shape (i.e. Dashidaira reservoir, Japan),

small disturbance in the inflow condition is very likely to change the flow pattern and subsequently different erosion and deposition pattern would occur. Due to the high probability of disturbance in the inflow condition within a flushing event, accurate modeling of flushing channel size, shape and location in prototype scale would be difficult.

3- Meyer-Peter-Muller bed load transportation formula was employed for flushing simulation in Dashidaira reservoir. The numerical model could simulate the volume of the flushed out sediment with an appropriate accuracy. The simulated volume of flushed out sediment was underestimated about 25%. The reason is very low erosion rate in areas close to the dam and also far upstream of the reservoir. In areas close to the dam, complex flow field emerges because of the reservoir geometry. Besides, water level drawdown procedure is simplified in the numerical model compared to the reality. Thus, transport capacity was small in this region. Regarding the far upstream area, bed material type is coarse sediment and model could not represent the erosion pattern properly since the flow field simulation over such kind of material is complex. The complexity further magnifies when the accelerated shallow flow condition emerges. As an overall conclusion, numerical results disclosed that secondary currents have been overestimated which result in deeper erosion pattern along the outer part of the channel bending whereas smaller erosion is obtained for the inner part. Inaccuracies also could be attributed to the bed forms (i.e. dunes and anti-dunes) that have a significant effect on erosion pattern in numerical modeling. An empirical formula that is basically developed for small Froude numbers is used to represent the bed-forms in the model. Nevertheless, numerical model can predict an appropriate range for total volume of eroded sediment. Therefore, it would be possible to examine the effect of some measures on flushing efficiency for conducting more efficient sediment management strategies in this reservoir.

Acknowledgement

The authors would like to give their sincere thanks to Mr. Shuhei Minami from NEWJEC company for providing the data of Dashidaira reservoir in this study.

References

Adamson, A., Stovin, V. & Bergdahl, L. (2003): Bed shear stress boundary condition for storage tank sedimentation. Journal of Environmental Engineering, ASCE, Vol. (129), No. 7, pp. 651-658.

Atkinson, E., (1996): The feasibility of flushing sediment from reservoirs, Tech. report, HR Wallingford, UK.

Batuca, D. G. and Jordaan, J.M. (2000): Stilling and desilting of reservoirs, A. A. Balkema, Rotterdam.

Chandler, K., Gill, D., Maher, B., Macnish, S. and Roads, G. (2003): Cooping with maximum probable flood-an alliance project delivery for Wivenhoe Dam, Proceedings of 43rd conference, Hobart, Tasmania.

Chiang, T. P., Sheu, T.W.H. & Wang, S. K. (2000): Side wall effects on the structure of laminar flow over plane symmetric sudden expansion. Computers & Fluids, Vol. (29), No. 5, pp. 467-492.

Chu, V. H., Wu, J-H. & Khayat, R. E. (1991): Stability of transverse shear flows in shallow open channels, Journal of Hydraulic Engineering, ASCE, Vol. (117), No. 10, pp. 1370-1388.

Dewals, B. J., Kantoush, S. A., Erpicum, S., Pirotton, M. & Schleiss, A. J. (2008): Experimental and numerical analysis of flow instabilities in rectangular shallow basins, Environmental fluid mechanics, Vol. (8), No. 1, pp. 31-54.

Dufresne, M., Dewals, B., Erpicum, S., Archambeau, P. & Pirotton, M. (2011): Numerical investigation of flow patterns in rectangular shallow reservoirs, Engineering Application of Computational Fluid Mechanics Vol. (5), No. 2, pp. 247-258.

Esmaeili, T., Sumi, T. & Kantoush, S. A. (2014): Experimental and numerical study of flushing channel formation in shallow reservoirs, Annual Journal of Hydraulic Engineering, JSCE, Vol. (70), No. 4, pp. I19-I24.

Frey, P., Champagne, J. Y., Morel, R. & Gay, B.

(1993): Hydrodynamics fields and solid particle transport in a settling tank. Journal of Hydraulic Research, Vol. (31), No. 6, pp. 736-776.

Ghidaoui, M. S. & Kolyshkin, A. A. (1999): Linear stability of lateral motions in compound open channels. Journal of Hydraulic Engineering, ASCE, Vol., (125), No. 8, pp. 871-880.

Haun, S. and Olsen, N. R. B. (2012): Three-dimensional numerical modeling of reservoir flushing on a prototype scale, Int. J. River Basin Management, Vol., (10), No. 4, pp. 341-349.

Haun, S., Dorfman, C., Harb, G. and Olsen, N. R. B. (2012): 3D numerical modeling of the reservoir flushing of the Bodendorf reservoir, Austeria, Proceedings of IAHR European conference, Munich, Germany.

Kantoush, S. A., Sumi, T. & Schleiss, A. J. (2010a): Geometry effect on flow and sediment deposition pattern in shallow basins. Annual Journal of Hydraulic Engineering, JSCE, Vol. (54), pp. 212-232.

Kantoush, S. A., Sumi, T., Suzuki, T., and Murasaki, M. (2010b): Impacts of sediment flushing on channel evolution and morphological processes: Case study of the Kurobe River, Japan, Proceedings of 5th River Flow Conference, Germany, Braunschweig.

Kantoush, S. A., Bollaert, E. & Scleiss, A. J. (2008a): Experimental and numerical modelling of sedimentation in a rectangular shallow basin. International Journal of Sediment Research, Vol. 23, No. 3, pp. 212-232.

Kantoush, S. A., De Cesare, G., Boillat, J.L. & Schleiss, A. J. (2008b): Flow field investigation in a rectangular shallow reservoir using UVP, LSPIV and numerical modeling. Flow Measurement & Instrumentation, Vol. (19), pp. 139-144.

Kantoush, S. A. (2007): Symmetric or asymmetric flow patterns in shallow rectangular basins with sediment transport. Proceedings of 32rd IAHR Congress, Venice, Italy.

Khosronejad, A., Rennie, C.D., Salehi Neyshabouri, A.A. and Gholami, I. (2008): Three dimensional numerical modeling of sediment release, Journal of Hydr. Research, Vol. (46), No. 2, pp. 209-223.

Launder, B.E. and Spalding D. B. (1972): Lectures in Mathematical Models of Turbulence, Academic Press, London.

Liu, J., Minami, S., Otsuki, H., Liu, B. and Ashida, K. (2004): Prediction of concerted sediment flushing, Journal of Hydr., Eng., ASCE, Vol. (130), No. 11, pp. 1089-1096.

Minami, S., Noguchi, K., Otsuki, H., Fukuroi, H., Shimahara, N., Mizuta, J. and Takeuchi, M. (2012): Coordinated sediment flushing and effect verification of fine sediment discharge operation in Kurobe River, Proceedings of the International symposium on dams for changing world, ICOLD, Kyoto, Japan.

Morris, G. L. and Fan, J. (1998): Reservoir Sedimentation Handbook: Design and Management of Dams, Reservoirs and Watersheds for Sustainable Use, McGraw-Hill, New York.

Olsen, N. R. B., (2011): A three-dimensional numerical model for simulation of sediment movements in water intakes with multiblock option, www.ntnu.no, Online User's manual.

Patankar, S.V. (1980): Numerical Heat Transfer and Fluid Flow, McGraw-Hill, New York.

Public Works Research Institute of Ministry of Construction (PWRI) (1993): The property and planning of the channel in Kurobe river (in Japanese).

Shapira, M., Degani, D. & Weihs, D. (1990): Stability and existence of multiple solutions for viscous flow in suddenly enlarged channels, Computers & Fluids, Vol., (18), No. 3, pp. 239-258.

Stovin, V. R. & Saul, A.J. (1996): Efficiency prediction for storage chambers using computational fluid mechanics. Water Sciences & Technology, Vol. (33), No. 9, pp. 163-170.

Sumi, T., 2006: Reservoir sediment management measure and necessary instrumentation technologies to support them, The 6th Japan-Taiwan Joint Seminar on Natural Hazard Mitigation.

Van Rijn, L. C. (1984a): Sediment transport. Part I: Bed load Transport, Journal of Hydraulic Engineering, ASCE, Vol. (110), No. 10, pp. 1733-1754.

Van Rijn, L. C. (1984b): Sediment transport. Part II: Suspended load Transport, Journal of Hydraulic Engineering, ASCE, Vol. (110), No.

11, pp. 1431-1456.
Van Rijn, L. C. (1984c): Sediment transport. Part III: Bed forms and alluvial roughness, Journal of Hydraulic Engineering, ASCE, Vol. (110), No. 12, pp. 1733-1754.
Yuce, M. I. & Chen, D. (2003): An experimental investigation of pollutant mixing and trapping in shallow costal re-circulating flows. Proceedings of International Symposium on Shallow flows, Balkema, Delft, Netherlands.

(Received June 10, 2014)